

Numerical and Experimental Analysis of Welding Deformation in Thin Plates

M.R. Khoshravan¹ and M.A. Setoodeh¹

Abstract: The use of welding to permanently join plates is common in industry due to its high efficiency. But welding creates thermal stresses, which can lead to residual stresses and physical distortion. This phenomenon directly influences the buckling stiffness of the welded structure. The welding distortion not only makes difficult the erection of the project, but also influences the final quality and cost of production. In this research, the thermo-elastic-plastic conditions were simulated by a three-dimensional (3D) finite element model (FE). Mechanical and thermal properties of the material were applied to the model, leading to eigenvalue analysis of the thermal and longitudinal stress distribution, buckling during welding and global. The research was performed on thin plates welded by butt joints and T-joints. A birth and death method depending on time was also used to model the molten pool. Since welding is a thermo-mechanical process, a coupling method was used to obtain results for nonlinear transient thermal analysis and introduce them in the structure analysis in order to investigate the buckling phenomenon. A comparison of our numerical results with those obtained from our experiments showed that the models can help predict when and where local buckling can occur. This method can also help predict the heat distribution and deformation during and after welding.

Keywords: Welding, Buckling, Three-dimensional finite element, Distortion, thin plate, residual stress

1 Introduction

Welding creates thermal stresses in the plate that lead to distortion and residual deformation in the welded structure following which the buckling stiffness decreases considerably. The main reason for the appearance of these distortions after welding is the creation of residual stresses. These stresses have an important role in the mechanical performance of structures. For example, high values of tensional

¹ University of Tabriz, Faculty of Mechanical Engineering, 51666, Tabriz, Iran

residual stress lead to possible rupture and decreased fatigue life in welded joints. Residual compression stresses can lead to global buckling or undesired local buckling during or after welding. These deformations are higher in thin plates. Methods to predict and prevent these distortions would be helpful. Distortion resulting from welding can be divided into six categories: transverse shrinkage, angular distortion, rotational deformation, longitudinal shrinkage, bending distortion and buckling distortion.

Buckling is a distortion that occurs suddenly and without any early warning. Methods of welding metals are different depending on the base metal. Distortions caused by welding are highly influenced by the welding speed, the welding manner the choice of electrode, and the voltage and current density. A convenient method for proper use of these parameters is important [American welding society (1991)]. The heat resulting from the welding arc constitutes about 40% of the total heat, and the heat resulting from the melted metal constitutes the other 60%. The choice of a conventional method of thermal simulation that considers all the related parameters and the quantity of applied heat in the weld is important in modeling.

Bonifaz (2000) obtained the reachable energy of an electrode by using thermal efficiency. He also obtained the temperature distribution by taking into account the relationship in heat transfer of the ratio of incoming energy per unit of surface, the ratio of incoming energy per unit of time and the effective conductional heat transfer.

Sarkani et al (2000) compared results of residual stresses in 2D and 3D modeling in T-joints. They concluded that there was a 30% difference between them.

Antonio et al (2005) evaluated heat propagation in the time domain generated by transient heat sources placed in the presence of three-dimensional media. Their evaluation required the use of computationally demanding numerical schemes. The implementation of numerical 3D solutions benefited from the existence of benchmark solutions to test the accuracy of approximate schemes.

Zhu and Chao (2002) studied the influence of material properties on the transient heat transfer, residual stresses and resulting distortion. They reached to their objective by using thermo-mechanical analysis and 3D nonlinear transient thermal analysis with FE methods. They reached four conclusions:

1. The coefficient of heat conductivity influences the transient heat distribution during welding.
2. In analysis of heat distribution in welding, the influence of density and specific heat capacity can be neglected.

3. The yield stress is a key property in the simulation of welding, and its value influences the residual stresses and resulting distortion.
4. The Young modulus and thermal dilatation coefficient have less influence relative to the other cited parameters in the creation of residual stresses and distortions.

Other works have been developed in the field of thermal stress and heat conductivity [Chang et al (2010)].

Divo and Kassab (2005) reviewed the dual reciprocity boundary element method for linear diffusion and proposed an approach to solve non-linear diffusion problems. They also provided an error estimator. Numerical results provided confidence in the approach and indicated that the error estimator was able to predict the temporal trend of the exact error at different discretization levels.

Wu et al (2007) used the new and advanced method of DE-GMAW. They analyzed heat distribution, residual stresses and distortion by heating modeling and experiments. They used two heat sources to generate principal and secondary currents. The secondary current was for preheating of welding metal and the piece. The principal current performed the welding operation. They demonstrated that this method has some advantages like increasing the filler metal deposit ratio, decreasing the introduced heat to the piece and decreasing residual stresses and deformation. Also by increasing the welding speed, a higher quality of welding could be created.

Modeling in 2D differs from reality due to the neglecting of the longitudinal temperature gradient, which creates a local effect in temperature distribution [Masubuchi (1980)]. The longitudinal temperature gradient should not be neglected. This temperature gradient influences the temperature distribution in the piece, leading to errors between 2D numerical results and experiments.

Mollicane et al (2006) simulated the distortion by a thermo-elasto-plastic method. They tried to find a simple modeling by FE to compute the distortion in butt joint and T-joint welds. Their results showed that by increasing the longitudinal stresses in the length of the piece, bending and buckling also increased, with a notable part of the distortion occurring in the width of plate in the shape of an angle variation.

In the same way, several authors have developed the elastic and plastic behavior of the sheet [Xu et al (2008) and Liu, D.S. (2009)].

Sharifi and Gakwaya (2006) studied classes such as elastic, elasto-plastic, visco-elastic and visco-plastic in small deformation and elasto-plastic, hyper elastic, hyper plastic, hyper visco-elastic, and hyper visco-plastic in large deformation.

Asle Zaeem et al (2007) analyzed the global and local buckling of aluminum sheets using three-dimensional FE modeling in T-joints. They simulated the welding pro-

cess and demonstrated the validity of their results by experiments.

Deng and Murakawa (2008) analyzed the great distortions and residual stresses, as well as the manner of plastic strain distribution on thin plates in T-joints by using three-dimensional FE modeling, applying thermo-elasto-plastic conditions and using a volumetric heat source as proposed by Goldak and cited in Ref. [Masubuchi K. (1980)]. They proved that the molten metal flow has a notable influence on the temperature distribution and the shape of the welding zone. They showed that without taking into account the influence of the molten metal flow, higher temperature would be created in welding zone.

In recent years, the computational method was extended by several authors into 2D and 3D stress analysis [Mishuris et al (2006) and Liu, C.H. (2009)].

As indicated by the cited references and different techniques used in modeling of welding, it is necessary to develop a 3D analysis in residual stress and distortion due to welding and prove results by experiments.

2 Finite element modeling

Due to the local and concentrated heat resulted from welding and the rate of cooling, residual stresses are created in the specimen. In the simulation of welding, the influence of thermal and mechanical behavior on the specimen should be taken into account. Thus, we performed the FE simulation of welding by using the elasto-plastic relationship, accounting for the flow of material around the welding zone, applying the appropriate boundary conditions on the model and considering the heat transfer relationships. This method works well for non-linear analysis of the problem, and the treatment of the complex geometry.

Different steps of the FE analysis are shown on Fig. 1 [Teng T.L. et al (2001)]. In Fig. 2, dimension and the support points of the FE model are showed.

2.1 Thermal model

Performance of thermal analysis is based on heat transfer relationships, thermo-physical properties and the moving heat source. One of the important points in the simulation of the weld is the modeling of the heat source [Eslami M.R. et al (2009)].

One method used in this research is the method of concentrated loads, which is applied to the nodes of a volume. This method can be useful when using the technique of birth and death of an element. In this method, when the elements corresponding to the filler metal deposit are generated, we choose the corresponding nodes and apply to them a concentrated temperature load equal to the fusion point of the metal, Fig. 3 [Janosch, J. (2008)].

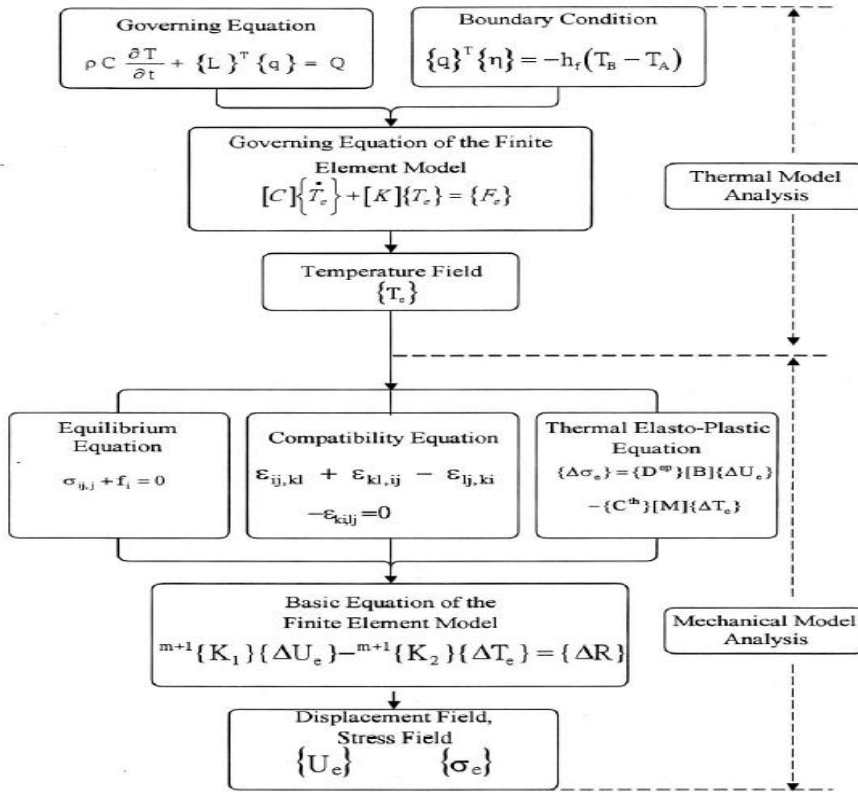


Figure 1: Flow chart of thermal and mechanical analysis steps [Teng T.L. et al (2001)]

This method has also been used in the heating modeling of this research.

2.1.1 Birth and death method

During analysis containing multiple loading, it is required to add or subtract some mass to the system. In the welding process, mass varies with time, as the metal filler of the weld is put in the weld place [Goldak J.A. (2005)]. In this kind of problem, the operator cannot add or subtract an element to the model after starting. By doing so, all the preceding loadings and their results would be destroyed and resolution of a new problem would be started. In these cases, the technique of birth and death is used to deactivate or activate again, the studied elements. The birth and death element method can be used in most of statically and non-linear transient analysis. To access to the particularity of birth and death of element, the

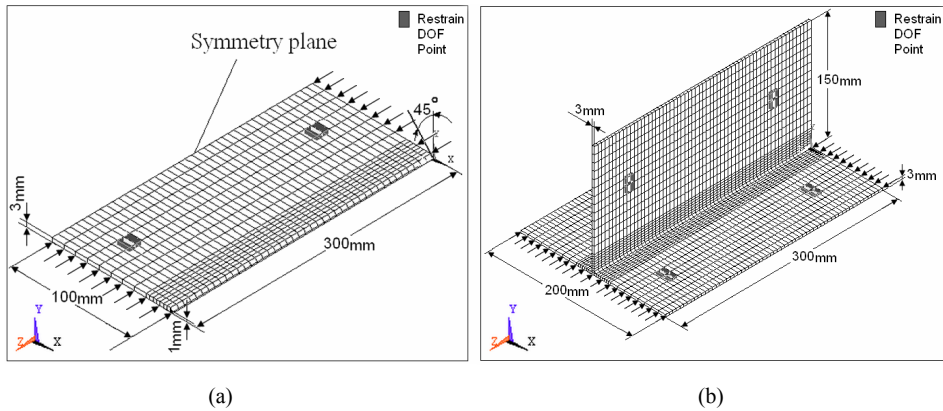


Figure 2: Dimensions of FE model in Butt-joint (a) and T-joint (b) welding analysis

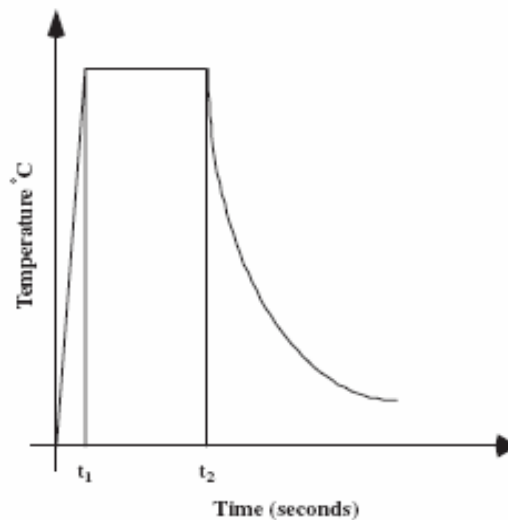


Figure 3: Input heat source [Janosch, J. (2008)]

death elements should not be completely deleted. They should be deactivated by crossing the stiffness matrix, heat transfer or other similar quantities in a very little reducing coefficient. In the first assumptions the value of the coefficient is 10^{-6} . But other value could be affected for inactive elements.

The loads of element, mass, attenuation, specific thermal coefficient and other effects are approximately zero. In a similar manner, when the elements are burned,

they are not added to the model, but are reactivated. When an element is reactivated, its stiffness, mass, elements load and others are returned to their initial values. The burned elements have kept any history of their supported strains. This method has been used in the modeling of welds in this research.

In some cases, the existence or nonexistence of elements of the model could be evaluated by the software on the basis of results of resolution. In the thermal-structure analysis of the welding, the element which are situated in liquid phase, should be inactivated is structural resolution. Then by time speeding and heat transfer and transformation of those element from liquid phase to solid, they are reconsidered in the structural analysis.

2.1.2 Heat transfer

The first attempt to reach the basic knowledge for design, heat and mechanical analysis of weld, is the precise evaluation of the transient temperature area. Some difficulties such as distortion, residual stresses, cooling rate, high temperature and stiffness decreasing in the welding zone and neighboring area result directly from the complex thermal cycle in welding zone. Therefore it is needed to study the manner of heat transfer during welding.

The following fundamental relations have been used in transient heat transfer analysis during welding [Deng and Murakawa (2008)].

$$\rho c \frac{\partial T}{\partial t}(x, y, z, t) = -\nabla \cdot q(x, y, z, t) + Q(x, y, z, t) \quad (1)$$

In which $\rho(g/mm^3)$ is the density, $c(J/g^\circ C)$ is the specific heat capacity, $T(^\circ C)$, $t(s)$ is the time, $q(w/mm^2)$ is the thermal flux vector, ∇ is the thermal gradient and $Q(w/mm^3)$ is the rate of internal produced heat.

The relation of the nonlinear isotropic heat flux is:

$$q = -k\nabla T \quad (2)$$

In this relation $k(J/mms^\circ C)$ is the heat conductivity coefficient dependent of temperature.

In heat modeling, application of heat transfer boundary conditions from the surface of the work piece is important. Coefficients of convection and radiation heat transfer are sensitive to temperature variation and should be applied variable with temperature.

Table 1 shows temperature depending properties of SUS 304 sheet that was used in this research.

Table 1 : Temperature depending properties of SUS 304 sheet [Deng and Murakawa (2006)]

Temperature (°C)	Specific Heat (J/g °C)	Conductivity (J/mm °C s)	Density (g/mm ³)	Yield Stress (MPa)	Thermal expansion coefficient (°C ⁻¹)	Young's modulus (GPa)	Poisson's ratio
0.0000	0.462	0.0146	0.790	265.00	1.70 e-5	198.50	0.294
100.00	0.496	0.0151	0.788	218.00	1.74 e-5	193.00	0.295
200.00	0.512	0.0161	0.783	186.00	1.80 e-5	185.00	0.301
300.00	0.525	0.0179	0.779	170.00	1.86 e-5	176.00	0.310
400.00	0.540	0.0180	0.775	55.00	1.91 e-5	167.00	0.318
600.00	0.577	0.0208	0.766	149.00	1.96 e-5	159.00	0.326
800.00	0.604	0.0239	0.756	91.00	2.02 e-5	151.00	0.333
1200.0	0.676	0.0322	0.737	25.00	2.07 e-5	60.00	0.339
1300.0	0.692	0.0337	0.732	21.00	2.11 e-5	20.00	0.342
1500.0	0.700	0.120	0.732	10.00	2.16 e-5	10.00	0.388

Relation of heat transfer by convection was obtained by the rule of Newton and its global Equation is as follow [Deng and Murakawa (2008)]:

$$q_C = -h_f (T_{sur} - T_0) \quad (3)$$

In which $h_f(w/mm^2 \text{ } ^\circ C)$ is the coefficient of convection, $T_{sur}(^\circ C)$ is the surface temperature and $T_0(^\circ C)$ is the ambient temperature.

Also the relation of heat transfer by radiation was obtained by the rule of Stephen-Boltzman and its global Equation is as follow [Deng and Murakawa (2008)]:

$$q_r = \varepsilon \sigma (T_{sur}^4 - T_0^4) \quad (4)$$

In which ε is the coefficient of radiation and σ is the constant of Stephen-Boltzman for radiation.

As the coefficient of convection depends on temperature, Eq. (5) has been used. Thus we have [Deng and Murakawa (2006)]:

$$h = \begin{cases} 0.68T \times 10^{-7} (w/mm^2) & 0 < T < 500^\circ C \\ (0.231T - 82.1) \times 10^{-6} (w/mm^2) & T > 500^\circ C \end{cases} \quad (5)$$

In which $T(^\circ C)$ is the temperature. This equation calculates the sum of both effects of heat transfer basing on temperature zone and gives precise results. Therefore they were used in our analysis.

2.1.3 Governing equations in thermal analysis

The following heat transfer relations based on enthalpy [Teng T.L. et al (1998)] have been used in this research.

For a volume of control which is bounded by an arbitrary surface; the fundamental equation of heat conduction is:

$$\rho C \frac{\partial T}{\partial t} = \{L\}^T ([D] \{L\} T) + Q = \frac{\partial}{\partial x} \left(K_x \frac{\partial T}{\partial x} \right) + \frac{\partial}{\partial y} \left(K_y \frac{\partial T}{\partial y} \right) + \frac{\partial}{\partial z} \left(K_z \frac{\partial T}{\partial z} \right) + Q \quad (6)$$

and the boundary condition of heat convection over the control volume surface is

$$\{q\}^T \{\eta\} = -h_f (T_B - T_A) \quad (7)$$

where ρ is density, C is specific heat, T is temperature, t is time, $\{q\}$ is heat flux, Q is the rate of internal heat generation, η is the unit outward normal vector, h_f is

the film coefficient, T_B is the bulk temperature of the adjacent fluid, and T_A is the temperature at the surface of the model.

Pre-multiplying the governing equation by a virtual change δT , integrating over the volume of the element and considering the boundary condition, Eq. (6) yields

$$\int_V (\delta T \rho C \frac{\partial T}{\partial t}) dV + \int_V (\delta T \{L\}^T [D] \{L\} T) dV = \int_V (\delta T Q) dV + \int_A (\delta T h_f (T_B - T_A)) dA \quad (8)$$

The variable T is allowed to vary in both space and time; Eq. (8) can be expressed as

$$\rho \int_V (C [N] [N]^T \{ \dot{T}_e \}) dV + \int_V ([B]^T [D] [B] \{ T_e \}) dV = \int_A [N] Q dV + \int_V [N] h_f (T_B - [N]^T \{ T_e \}) dA \quad (9)$$

Where $[N]$ are element shape functions, and $\{ T_e \}$ is the nodal temperature vector.

Eq. (9) can be rewritten as:

$$[C] \{ \dot{T}_e \} + [K] \{ T_e \} = \{ F_e \} \quad (10)$$

In which

$$\begin{aligned} [C] &= \rho \int_V C [N]^T [N] dV \\ [K] &= \int_V [B]^T [D] [B] dV + \int_A h_f [N] [N]^T dA \\ \{ F_e \} &= \int_V Q [N] dV + \int_A h_f T_B [N] dA \end{aligned} \quad (11)$$

The temperature field in thermal model analysis may be obtained from Eq. (10). Those results are then inserted into the mechanical model.

2.2 Mechanical model

Welding is a thermo-mechanical phenomenon. Therefore FE analysis of welding consisted of two steps. First Thermal analysis using FE should be carried out. Then, by applying the obtained results on the mechanical model, the mechanical analysis is performed.

2.2.1 General principles

For a precise resolving of a structural problem in order to obtain stresses, three principal rules should be respected. They consist of equilibrium equations, stress-strain relations and compatibility relations between strains and displacements. In addition, predetermined boundary conditions (BC) of displacements and other necessary BC should also be respected.

Globally, in the FE analysis of stress, the model is obtained by a system of equilibrium equation resulted by discretization of the virtual work relation. Until the step that the problem of weld analysis depends on the history, resolving of the system of equilibrium equations, from the beginning of process to the final cooled temperature, is performed in a set of small elements. In each element the nodal deformations are computed by Newton iteration method or other numerical methods. In the term of all iterations the variables of strain and stress are updated, and then the residual stress is calculated and compared with the variations of the load. The equilibrium resolution converges if the absolute maximum of all residual loads becomes lower than the indicated tolerance.

2.2.2 Governing equations in mechanical analysis

According to the principle of virtual work and the divergence theorem, the equilibrium equations and the constitutive equations can be rewritten in the matrix form as

$$\int_V \{\delta \boldsymbol{\varepsilon}\}^T \{\boldsymbol{\sigma}\} dV = \int_A \{\delta \boldsymbol{u}\}^T \{P\} dA + \int_V \{\delta \boldsymbol{u}\}^T \{f\} dV \quad (12)$$

Let

$$\begin{aligned} \{\boldsymbol{\varepsilon}\} &= [B] \{U_e\} \\ \{\delta \boldsymbol{\varepsilon}\} &= [b] \{\delta U_e\} \\ [B] &= [L] [N] \end{aligned} \quad (13)$$

Where $\{P\}$ is the surface force vector, $\{f\}$ is the body force vector, $\{u\}$ is the displacement vector, $\{\boldsymbol{\varepsilon}\}$ is the strain vector, $\{\boldsymbol{\sigma}\}$ is the stress vector, $\{U_e\}$ is the nodal displacement vector, $[B]$ is the strain- displacement matrix, $[N]$ is the matrix of shape function, and $[L]$ is the differential operator matrix.

Substituting Eq. (13) into Eq. (12) yields

$$\int_V [B]^T \{\boldsymbol{\sigma}\} dV = \{R\} = [K] \{U_e\} \quad (14)$$

Where $\{R\}$ and $\{K\}$,

$$\{R\} = \int_A [N]^T \{P\} dA + \int_V [N]^T \{f\} dV \quad (15)$$

$$\{K\} = \int_V [B]^T \{D^e\} [B] dV$$

are respectively the nodal equilibrium external force matrix, and the stiffness matrix.

The above expressions are assumed to represent a linear, elastic model. Since the nodal displacement functions are nonlinear functions in the elasto-plastic analysis, an incremental calculation is employed. For the incremental analysis, the load $\{R\}$ at step $(m+1)$ may be expressed as

$${}^{m+1}\{R\} = {}^m\{R\} + \{\Delta R\} \quad (16)$$

If the solution of ${}^m\{U_e\}$, ${}^m\{\sigma_e\}$, ${}^m\{\epsilon_e\}$ at the m^{th} step are assumed to be known, the solution of the $(m+1)^{th}$ step can then be obtain as

$${}^{m+1}\{U_e\} = {}^m\{U_e\} + \{\Delta U_e\} \quad (17)$$

$${}^{m+1}\{\sigma_e\} = {}^m\{\sigma\} + \{\Delta\sigma_e\}$$

Accordingly, Eqs. (14) and (16) become

$$\int_V [B]^T \{\Delta\sigma_e\} dV = {}^m\{R\} + \{\Delta R\} - \int_V [B]^T {}^m\{\sigma_e\} dV \quad (18)$$

Substituting Eq. (14) into Eq. (18) yields

$$\int_V [B]^T \{\Delta\sigma_e\} dV = \{\Delta R\} \quad (19)$$

The thermal elasto-plastic material model, based on the von Mises yield criterion and the isotropic strain-hardening rule, is considered. Stress-strain relation can be written as

$$\{\Delta\sigma_e\} = \{D^{ep}\} [B] \{\Delta U_e\} - \{C^{th}\} [M] \{\Delta T_e\} \quad (20)$$

and

$$\{D^{ep}\} = \{D^e\} + \{D^p\} \quad (21)$$

where $\{\Delta\sigma_e\}$ is the nodal stress increment matrix, $\{\Delta\varepsilon_e\}$ is the nodal strain increment matrix, $\{\Delta T\}$ is the temperature increment matrix, $\{D^e\}$ is the elastic stiffness matrix, $\{D^p\}$ is the plastic stiffness matrix, $\{C^{th}\}$ is the thermal stiffness matrix, $\{\Delta T_e\}$ is the nodal temperature increment matrix, and $[M]$ is the temperature shape function.

Substituting Eq. (20) into Eq. (19):

$${}^{m+1}\{K_1\}\{\Delta U_e\} - {}^{m+1}\{K_2\}\{\Delta T_e\} = \{\Delta R\} \quad (22)$$

Where

$${}^{m+1}\{K_1\} = \int_V [B]^T \{D^{ep}\} [B] dV \quad (23)$$

$${}^{m+1}\{K_2\} = \int_V [B]^T \{C^{th}\} [M] dV$$

The displacement increment $\{\Delta U_e\}$ and stress increment $\{\Delta\sigma_e\}$ can be obtained from Eqs. (20) and (22). With these results, the displacement $\{U_e\}$ and stress $\{\sigma_e\}$ are then obtained from Eq. (17).

3 Prediction of welding distortion

In the welding of thin plates, we observe great deformations that appear suddenly without any initial signal. These great deformations are called buckling.

The buckling phenomenon in welding is due to apparition of the huge compression stresses. They are the result of thermal stresses obtained by the complex temperature distribution on the work piece in remote area of the welding zone.

In the present research, in addition to the modeling, in order to predict and analyze the local buckling by using the elasto-plastic model and non-linear calculation depending on temperature during welding, we tried to analyze the global buckling of the piece after the weld was been cooled.

To predict the local buckling, we used a method in which the specifics of the sudden deformation were taken into account. So for the local buckling analysis during welding, the deformation of the plate during welding was not prevented. The point in which an important deformation based on elasto-plastic analysis was observed, the local buckling has been analyzed to know if buckling was occurred or no. For this reason, for the points for which the local buckling was the most probable in our knowledge, the time depending curves of stress and time depending curves of deformation were extracted from thermal and mechanical analysis. By comparing those curves, if in the time depending curve of deformation a great variation was

observed in a given time and at the same time there was not a clear variation in the time depending curve of stress, apparition of a local buckling on that point and on that time explained the phenomenon.

By using results of stress distribution and remained loads in the welded piece obtained by thermo-mechanical analysis, we performed a global buckling analysis in several chosen points after welding and making the structural model in the cooled piece.

The global buckling of welded structures has been analyzed by using the eigenvalue method (Euler classic). Analysis of eigenvalues corresponding to elastic instability is described by following equation [Asle Zaeem, M. et al (2007)].

$$\det(k + \lambda k_G) = 0 \quad (24)$$

In which k is the linear stress stiffness matrix, k_G is the non-linear stress stiffness matrix and λ is the eigenvalue. It is given by the following equation.

$$\lambda = \frac{\sigma_{cr}}{\sigma_l} \quad (25)$$

In which σ_{cr} is the critical stress of buckling, σ_l is the longitudinal stress obtained from the heat analysis and λ is the computed eigenvalue by software. Regarding Eq. (25), buckling will occur if $\lambda \leq 1$. It means when residual longitudinal stresses are higher than the critical buckling stress.

4 Experimental

The used plates were made of stainless steel SUS 304 with 3mm thickness. This kind of metal is used among many fields of industry for welded joints. Therefore, distortions occurring on these structures are a significant problem.

Dimensions of plates that were used in our experiments were chosen similar to those of modeling.

The TIG process, which is convenient for this kind of steel with the corresponding thickness, has been chosen for the welding method. Welding was carried out in voltage 220 Volts with a current rate 160 Amperes by applying DCEN polarity and with a welding speed 2.5 mm/s.

The temperature on the surface of plates was measured on the pre-selected points using two thermometers with a thermocouple wire of kind k. This apparatus functions in temperature range of 30°C to 1600°C. It can be branched too many kind of thermocouples such as PT-100, J, K, Ni, NiCr, Pt-Rapt and semiconductors.

To measure the distortion of the piece after welding a comparator with precision 0.1mm was used.

First the two heads of T-joint and butt joint were joint with a punctual welding. As in modeling, all of the surfaces are free to heat exchange with environment, in order to create similar conditions in modeling, except in the supporting points which are in contact with bushes to keep the structure upper than work table; all of other surfaces were kept free and in contact with their neighbor air.

To create supporting points in vertical sheet (web) of T-joint, by conception and making fixture apparatus, displacements of supporting points were stopped in all directions (x, y, z). Figures (4) and (5) show the manner of carrying of experiments and measuring of distortion in respectively butt-joint and T-joint.



Figure 4: Butt-joint welding set-up



Figure 5: T-joint welding set-up

5 Analyzing of experimental and modeling results

5.1 Butt-joint

Modeling of welding was performed with one pass, with a speed of 2.5 mm during 120 seconds (similar to the experimental part). Figure (6) shows the heat distribution and its influence on distortion of the piece during and after welding. Figure (6.a) shows the temperature distribution in the beginning of welding. This figure illustrates quite well the heat affected zone (HAZ) and the weld penetration.

In the experimental part, we checked the heat distribution in points one and two by measuring of temperature in different times using a thermometer, as presented in Fig. (7).

Obtained experimental results are presented in Fig. 8 and Fig. 9.

The curves of Fig. 8 and Fig. 9 proved that the evaluation of heat distribution on the surface of structure give the same results, either by experiments or numerical processing.

For the local buckling analysis during welding in the curve of distortion, if in a special time a pulse occurs without any modification in stress curve, it implies that a buckling event happens at that time and in that point.

We checked several points in situations on which buckling event were probable. We tried to study the local buckling in a desired point. The curves of distortion (Fig. 10) and stress (Fig. 11) are shown for the point six presented in Fig. 7.

As we observe in Fig. 10, at the time 90 seconds, there is a pulse of 0.02 mm in the curve of distortion. At the same time in the stress curve of Fig. 11, at that point there is not a pulse. The curve has a monotonic decreasing shape. Due to the mechanical properties of the metal, the occurred local buckling is not significant. This does not mean that local buckling occurs only on this point. It could happen in other points. Figures (12) and (13) show the manner of residual stress distribution in welding direction in different times.

In the supports application on the structure, there is a small compression along the entire surface of the structure. It is so weak, however, that it cannot cause buckling in the sheet without welding.

An increase in the length of the welding line causes the compression stresses along the welding gap line to also increase. In areas farther from the welding line, the compression stresses decrease and actually change to tensile stresses. In other words, the edges of the plate support a tensile stress. As the welding pat cools, the compression stresses in the weld cavity (where stress is highest) decrease and become tensile stresses. At the same time, the compression stresses move to the edges of plate. So in the end of cooling period, compression stresses will exist in the surface of the plate and tensile stresses will exist along the welding gap line.

Figure (14) shows the final distortion of the modeled plate after being cooled.

As shown in Fig. 14, after being cooled up to 600 seconds, distortion in both sides of the plate is symmetrical. In order to decrease the time and the volume of computation, the time length of computation was increased to 2523 seconds, but this caused an error in the software. The shape of distortion was changed from symmetrical to nonsymmetrical. The value of this error is not significant, however, and we can neglect it.

By performing buckling analysis using eigenvalues on the model and applying longitudinal stresses resulting from thermal analysis on the model, the eigenvalue resulting from analysis was 0.092. Following Eq. (25) and the comments that followed, we can conclude that since the eigenvalue is less than one, global buckling occurs on the plate.

Figure (15) shows the final distortion of the plate performed by experiment.

By measuring the value of distortion at different times at points three, four, and five

of the model as presented in Fig. 7 and measuring the value of distortion of the same points and same times in the experimental part, we can analyze the manner of final buckling of the plate. The points were chosen where buckling was most probable.

Table 2 presents results of both the numerical and experimental measurements.

We observe that the values of the measured distortion closely match those of the model.

5.2 T-joint

Welding in a T-joint was also modeled in one pass. Welding speed was 2.5 mm during 120 s. These conditions were similar to those used on experiments. Figure (16) shows the FE model accompanied with selected points for measurement.

Figure (17) shows the heat distribution and its influence on distortion of the piece during and after welding in T-joint welding. Figure (17.a) shows the temperature distribution at the beginning of welding. This figure illustrates the heat affected zone (HAZ) and the weld penetration.

We checked the heat distribution at points one and two as presented in Fig. 16. Obtained experimental results are presented in Fig. 18 and Fig. 19.

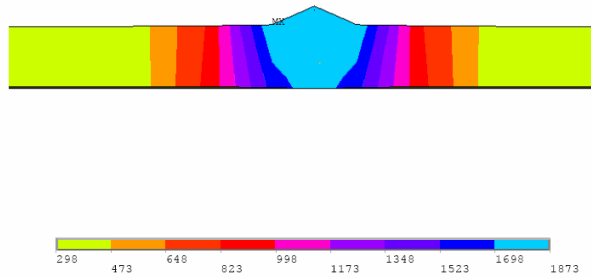
The curves of Fig. 18 and Fig. 19 show that the evaluation of heat distribution on the surface of structure give the same results from either experiments or numerical processing.

The curves of distortion (Fig. 20) and stress (Fig. 21) are shown for point six as presented in Fig. (16).

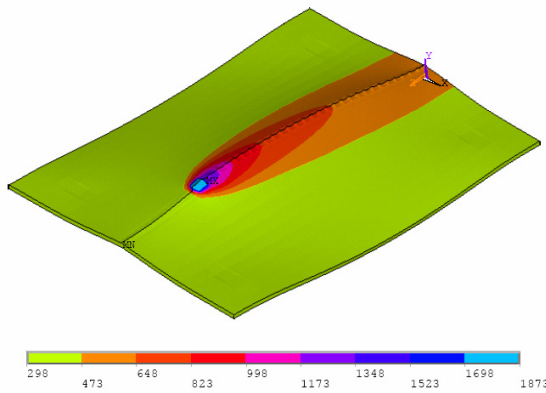
As we observe in Fig. 20, in the time 110 s, there is a pulse of 0.26 mm in the curve of distortion. At the same time in the stress curve of Fig. 21, at that point there is not a pulse. Due to the mechanical properties of the metal, the local buckling is not significant. Of course, the local buckling is not specific to this point. It could happen in other points as well. Figures (22) and (23) show the manner of residual stress distribution in welding direction in different times.

Table 2: Distortion value resulted by modeling and experimental

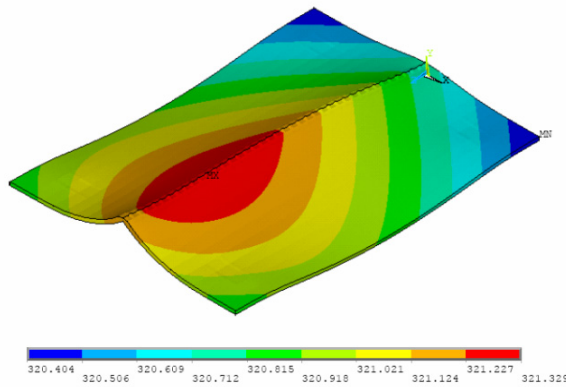
Distortion of point 5 (mm) experiment	analysis	Distortion of point 4 (mm) experiment	analysis	Distortion of point 3 (mm)		Time (s)
				experiment	analysis	
-1.22	-0.168	-1.23	-0.164	0.62	0.51	1020
-1.45	-0.169	-1.37	-0.164	0.55	0.503	1620
-1.63	-0.169	-1.55	-0.165	0.4	0.503	1920
-1.68	-0.17	-1.63	-0.165	0.34	0.503	2520



(a)



(b)



(c)

Figure 6: Temperature distribution. (a) at beginning of welding, (b) 90 s after beginning of welding, (c) 40 minutes after welding was finished.

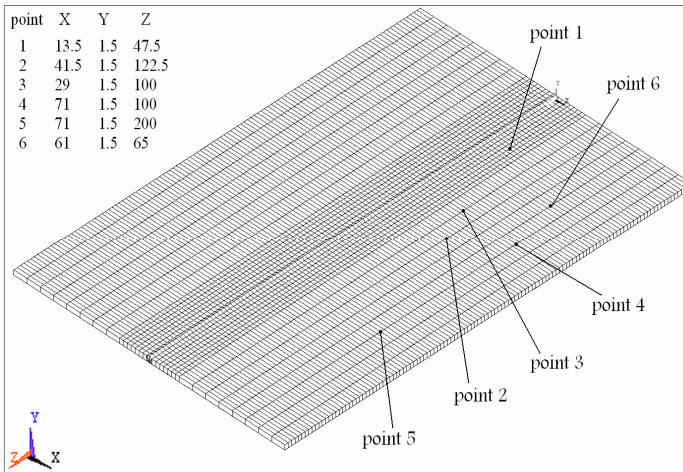


Figure 7: Coordinates of checkpoints in butt-joint model

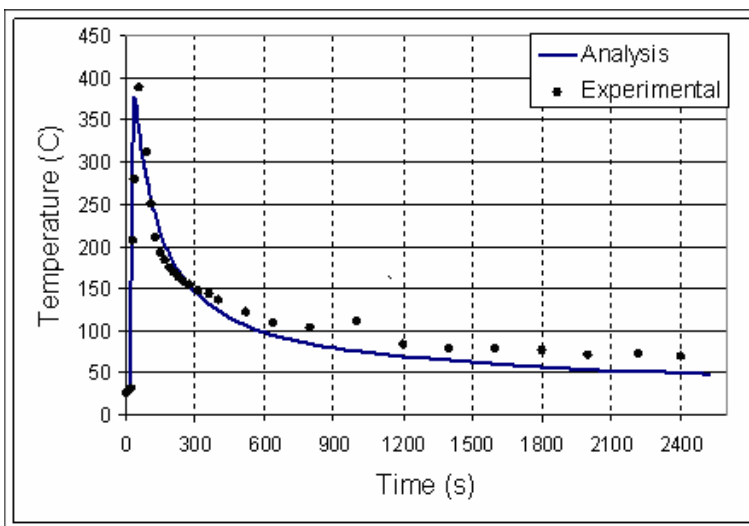


Figure 8: Heat distribution in point 1

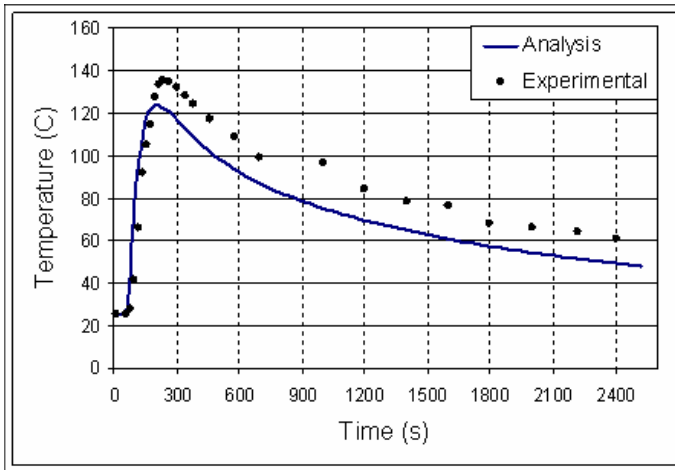


Figure 9: Heat distribution in point 2

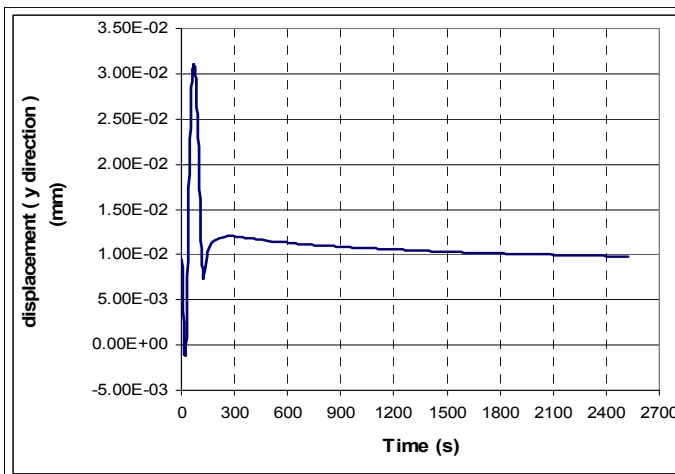


Figure 10: Curve of distortion versus time in point 6

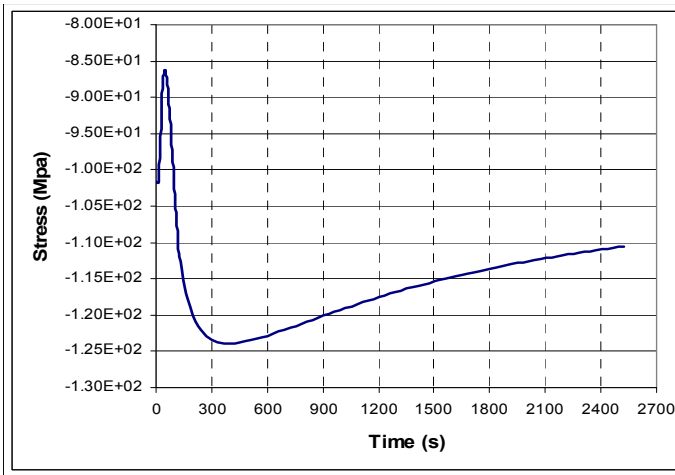


Figure 11: Curve of stress versus time in point 6

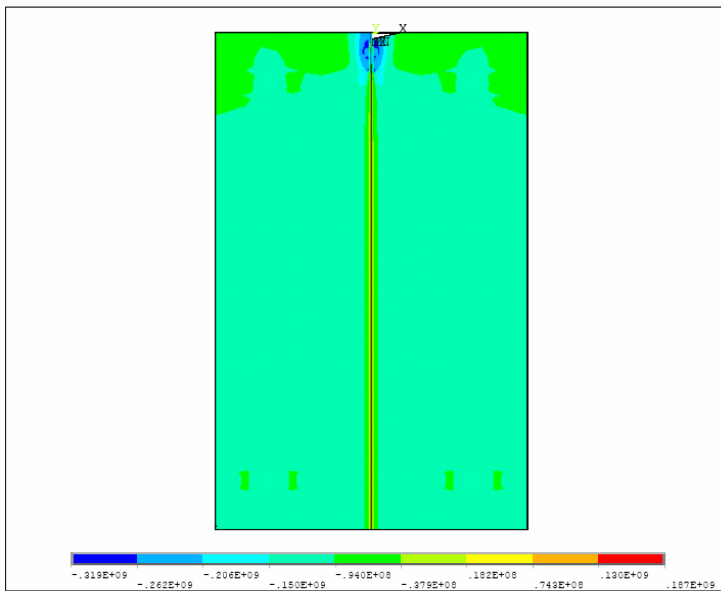
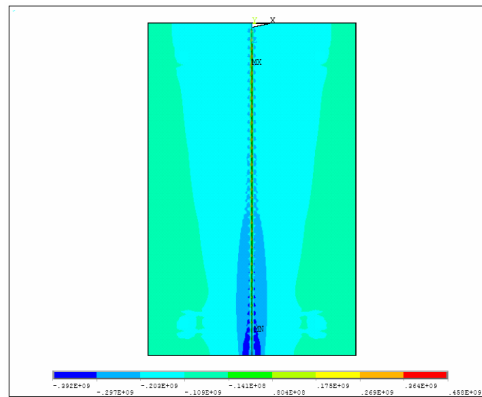
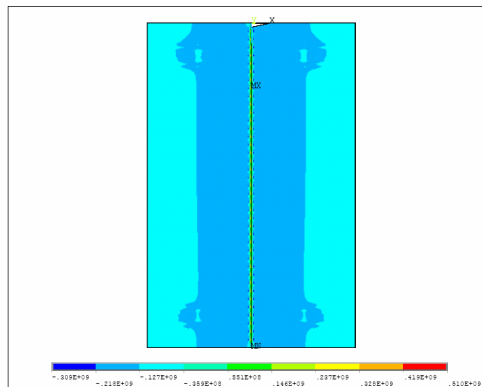


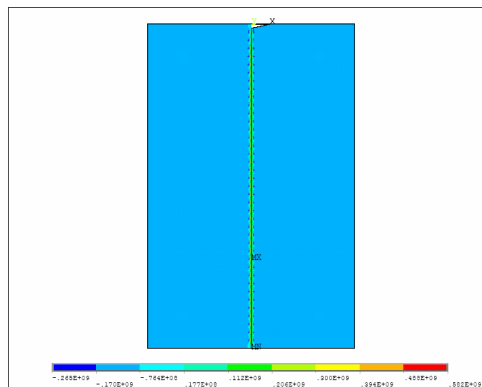
Figure 12: Residual longitudinal stress distribution during welding in Pa (9 s after the beginning of welding)



(a)



(b)



(c)

Figure 13: Residual longitudinal stress distribution during cooling in Pa at (a) 123 s, (b) 273 s and (c) 2523 s after beginning of welding

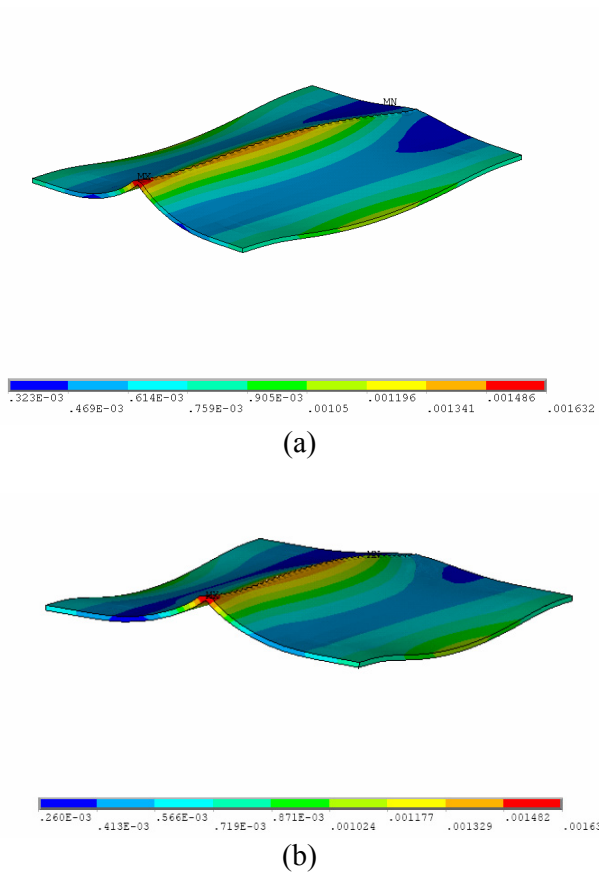


Figure 14: Final distortion of the modeled plate after (a) 600 s and (b) 2523 s of cooling



Figure 15: Final distortion of the plate performed by experiment

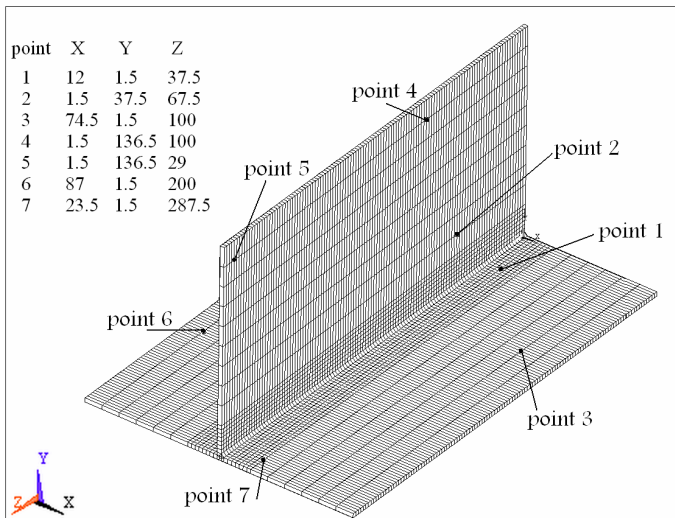


Figure 16: Coordinates of check points in T-joint model

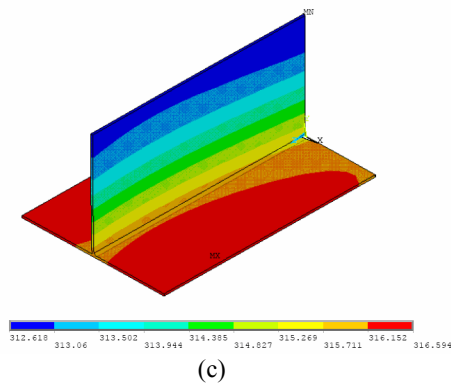
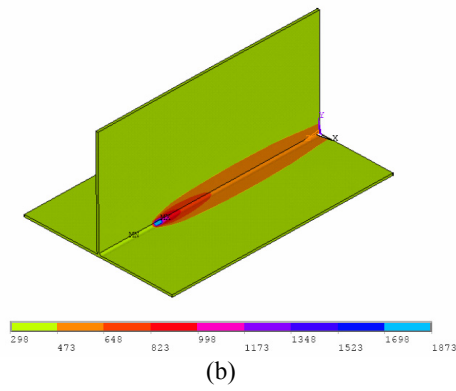
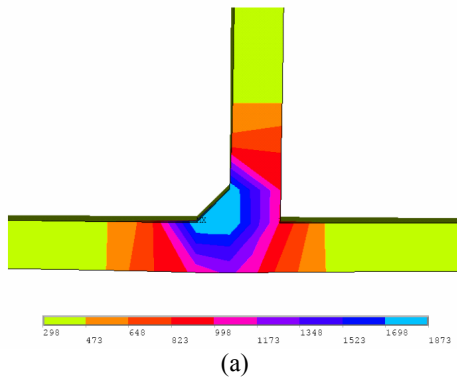


Figure 17: Temperature distribution. (a) at the beginning of welding, (b) 90 s after beginning welding, (c) 40 minutes after welding was finished.

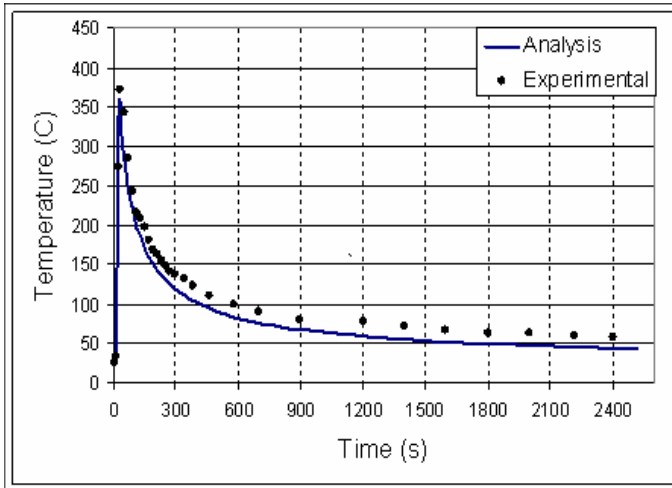


Figure 18: Heat distribution in point 1

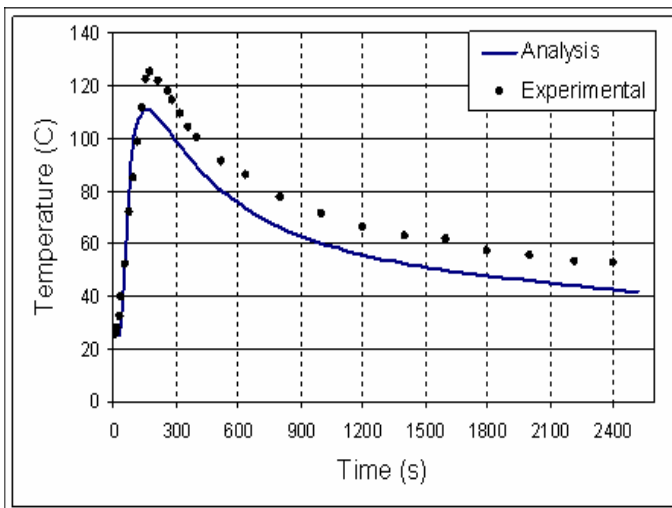


Figure 19: Heat distribution in point 2

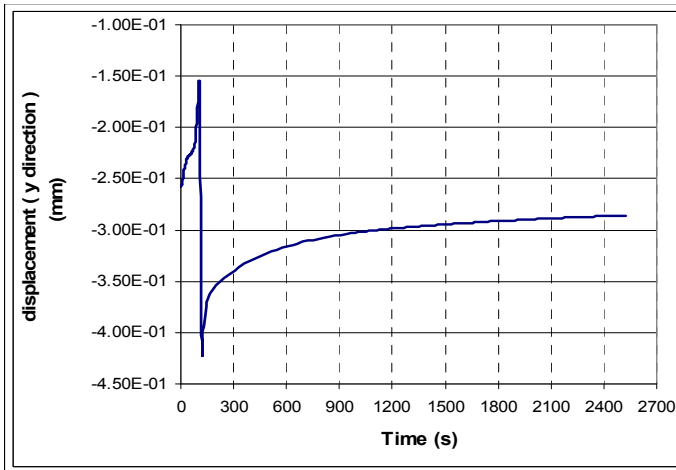


Figure 20: Curve of distortion versus time in point 6

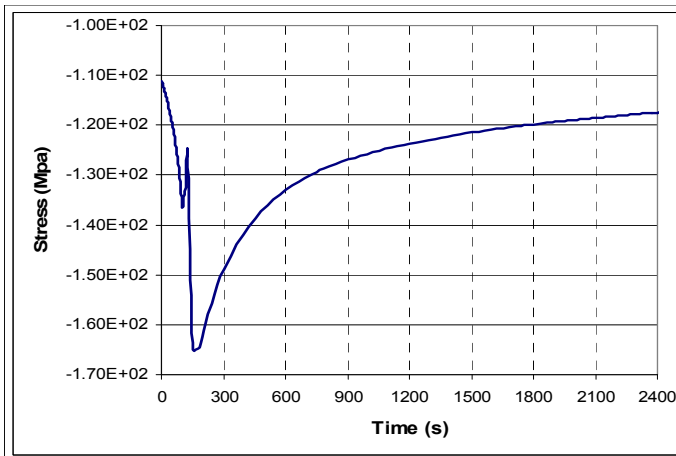
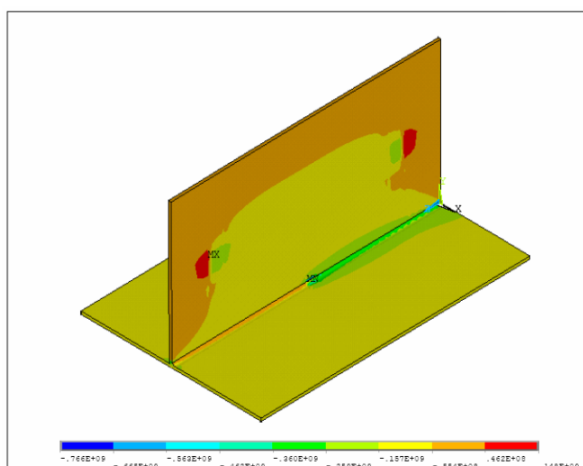
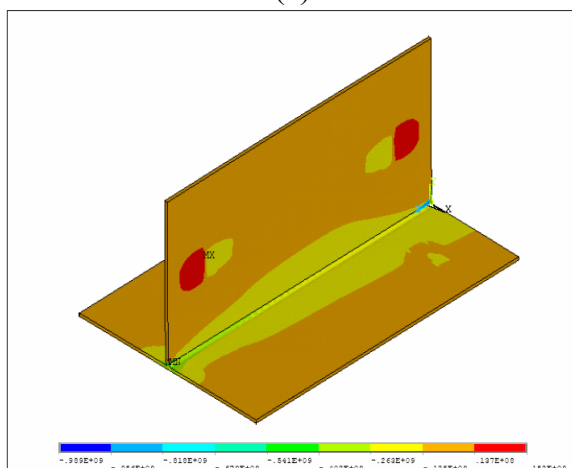


Figure 21: Curve of stress versus time in point 6



(a)

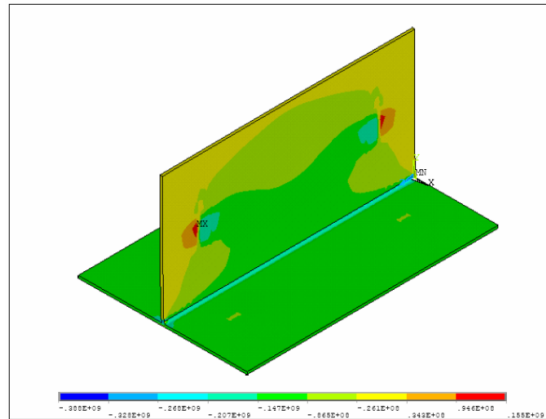


(b)

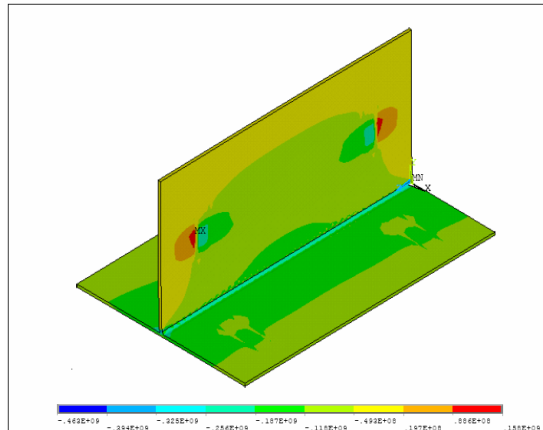
Figure 22: Residual longitudinal stress distribution during welding in Pa in times: (a) 60 s and (b) 120 s after the beginning of welding

In following of above-mentioned curves, the comments are similar to those of butt joints. Figure (24) shows the final distortion of the modeled plate after being cooled.

By performing an eigenvalue buckling analysis on the model and applying longitudinal stresses resulting from thermal analysis on the structural model, the obtained eigenvalue from analysis is equal to 0.166. Since this eigenvalue is less than one, we conclude that global buckling occurred on the piece. Figure (25) shows the final



(a)



(b)

Figure 23: Residual longitudinal stress distribution during cooling in Pa

distortion of the piece performed by experiment.

The values of distortion for points three, four, five, and six as illustrated in Fig. 16 was measured at different times using both the model and the experiment. These points were chosen because they were the most likely locations for buckling. The results of the modeled and experimental distortion are shown in Table 3. We can observe that the measured distortion is in accordance with results of modeling.

The results of Table 3 and other obtained results lead to the conclusion that our modeling and methods work well to predict buckling and evaluation of distortion in welded structures.

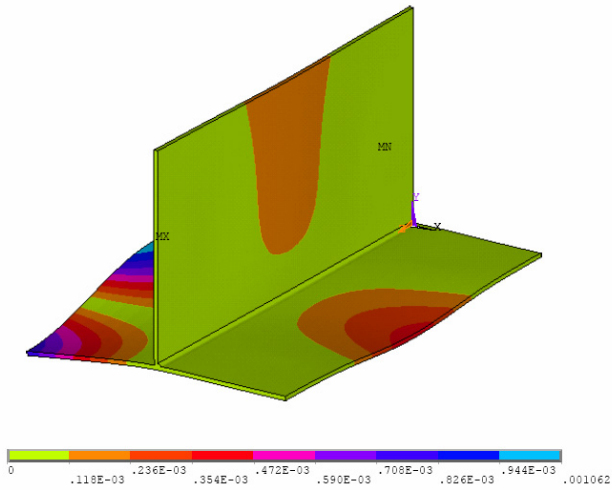


Figure 24: Final distortion of the modeled plate after being cooled



Figure 25: Final distortion of the plate performed by experiment.

Table 3: Values of distortion obtained by experiment and modeling

Distortion of point 4 (mm)		Distortion of point 3 (mm)		Time (s)
experiment	analysis	experiment	analysis	
-0.53	-0.235	-0.02	-0.023	720
-0.44	-0.232	-0.35	-0.023	1020
-0.38	-0.23	-0.38	-0.024	1620
-0.37	-0.229	-0.4	-0.024	1920
-0.35	-0.228	-0.4	-0.025	2520
Distortion of point 6 (mm)		Distortion of point 5 (mm)		Time (s)
experiment	analysis	experiment	analysis	
-0.63	-1.74	-0.02	-0.084	720
-0.98	-1.69	-0.05	-0.083	1020
-1.17	-1.65	-0.06	-0.082	1620
-1.22	-1.94	-0.05	-0.081	1920
-1.24	-1.62	-0.06	-0.08	2520

6 Conclusion

The analysis of our model and experiments lead to the following main conclusions:

1. Results obtained by modeling and numerical simulation are a good match with those obtained by experiments. The thermo-elasto-plastic model is an effective model to predict and analyze great distortions in welded structures.
2. The use of non-linear transient analysis in the model, applying temperature dependant properties, and applying the convection and radiation heat transfer conditions dependant on temperature led to results for heat and residual stresses with more precision than other models.
3. During cooling, longitudinal compressive stresses move from the welding zone to the edges of the plate and can cause buckling deformation in the area farthest from welding gap.
4. There is not much research on local buckling during welding, but the method used for local buckling analysis in our research can be effectively used for local buckling analysis during welding. The curves of distortion and stress illustrate that local buckling does not occur, due to the high stiffness of the material around the welding zone.
5. By applying the longitudinal stresses resulting from welding analysis on the model of a structure, using the eigenvalue method for global buckling analy-

sis after cooling and then comparing with experimental results, we conclude that the proposed modeling is efficient for the prediction of global buckling of a structure.

6. Our results demonstrate that the performed modeling is efficient for prediction and lowering of thermal stresses, distortions and buckling caused by welding in thin plates. It is helpful for decreasing the cost and design time of welded structures.

References

- American welding society** (1991): *Welding handbook*, Vol 4.8.
- Antonio, J., Tadeu, A., Godinho, L., Simoes, N.** (2005): Benchmark solutions for three-dimensional transient heat transfer in two-dimensional environments via the time Fourier transform. *CMC: Computers, Materials & Continua*, vol. 2, no. 1, 1-12.
- Asle Zaeem, M., Nami, M.R., Kadivar, M.H.** (2007): Prediction of welding buckling distortion in a thin wall aluminum T joint. *Journal of Computational Materials Science*, vol. 38, pp. 588-594.
- Bonifaz, E. A.** (2000): Finite element analysis of heat flow in single pass arc welds. *Welding Research Supplement*, pp.121s-125s.
- Chang, C.W., Liu, C.H., Chang, J.R.** (2010): A quasi-boundary semi-analytical approach for two-dimensional backward heat conduction problems. *CMC: Computers, Materials & Continua*, vol. 15, no. 1, 45-66.
- Deng, D. Murakawa, H.** (2006): Numerical simulation of temperature field and residual stress in multi-pass welds in stainless steel pipe and comparison with experimental measurements. *Journal of Computational Materials Science*. vol. 37, pp. 269-277.
- Deng, D. Murakawa, H.** (2008): Prediction of welding distortion and residual stress in a thin plate butt-welded joint. *Journal of Computational Materials Science*. vol.43, pp. 253-265.
- Divo, E., Kassab, A.J.** (2005): Transient non-linear heat conduction solution by a dual reciprocity boundary element method with an effective posteriori error estimator. *CMC: Computers, Materials & Continua*, vol. 2, no. 4, 277-288.
- Eslami, M.R., Hetnarski, R.B.** (2009): *Thermal Stress Advance Theory and Applications*, first ed., Springer, Netherlands.
- Goldak, J.A.** (2005): *Numerical analysis of welding mechanics*, Springer, NY10013, USA.

Janosch, J. (2008): International Institute of Welding work on residual stress and its application to industry. *International Journal of Pressure Vessels and Piping*. vol. 85, Issue 3, pp. 183-190.

Liu, D.S., Tsai, C.Y., Lyu, S.R. (2009): Determination of Temperature-Dependent Elasto-Plastic Properties of Thin-Film by MD Nanoindentation Simulations and an Inverse GA/FEM Computational Scheme. *CMC: Computers, Materials & Continua*, vol. 11, no. 2, 147-164.

Masubuchi, K. (1980): Analysis of welded structures. Oxford, pergamon press.

Mishuris, G., Chsner, O., Kuhn, G. (2006): FEM-analysis of non classical transmission conditions between elastic structures. Part 2: Stiff imperfect interface. *CMC: Computers, Materials & Continua*, vol. 4, no. 3, 137-152.

Mollicone, P., Camilleri, D., Gray, T.G.F., Comlekci, T. (2006): Simple thermo-elastic-plastic models for welding distortion simulation. *Journal of Materials Processing Technology*. vol. 176, pp. 77-86.

Sarkani, S., Tritchkov, V., Michaeliv, G. (2000): An efficient approach for computing residual stresses in welded joints. *Journal of Finite Element in Analysis and Design*. vol. 35, pp.247-268.

Sharifi, H., Gakwaya, A. (2006): Object-oriented modeling of solid material in nonlinear applications. *CMC: Computers, Materials & Continua*, vol. 3, no. 2, 77-96.

Teng, T.L., Chang, P.H. (1998): Three – dimensional thermomechanical analysis of circumferentially welded thin – walled pipes. *International Journal of Pressure Vessels and Piping*. vol. 75, pp. 237-247.

Teng, T.L., Fung, C.P., Chang, P.H., Yang, W.C. (2001): Analysis of residual stresses and distortions in T-joint fillet welds. *International Journal of Pressure Vessels and Piping*. vol. 78, pp. 523-538.

Wu, C.S., Zhang, M.X., Li, K.H., Zhang, Y.M. (2007): Numerical analysis of double-electrode gas metal arc welding process. *Journal of Computational Materials Science*. vol. 39, pp. 416-423.

Xu, L.M., Fan, H., Xie, X.M., C. Li, C. (2008): Effective elastic property estimation for bi-continuous heterogeneous solids. *CMC: Computers, Materials & Continua*, vol. 7, no. 3, 119-128.

Zhu, X.K., Chao, Y.J. (2002): Effects of temperature-dependent material properties on welding simulation. *Journal of Computers and Structures*. Vol. 80, pp. 967-976.